



# Model-based control of a 6-dof electrohydraulic Stewart–Gough platform

Ioannis Davliakos, Evangelos Papadopoulos \*

*Department of Mechanical Engineering, National Technical University of Athens, Athens 157 80, Greece*

Received 26 June 2006; received in revised form 26 November 2007; accepted 2 December 2007

---

## Abstract

In this paper, a novel model-based controller for a six Degree-of-Freedom (dof) electrohydraulic Stewart–Gough platform is developed. Dynamic models of low complexity are employed that describe the salient dynamics of the main electrohydraulic components. Rigid body equations of motion and hydraulics dynamics, including friction and servovalve models are used. The developed feedback controller uses the system dynamic and hydraulic model to yield servovalve currents, so that the error dynamics converge asymptotically to zero, independent of load variations. In this approach, force, pressure or acceleration feedback is not required. Simulations with typical desired trajectory inputs are presented and a good performance of the controller is obtained. The proposed methodology can be extended to electrohydraulic serial or closed-chain manipulators and simulators.

© 2007 Elsevier Ltd. All rights reserved.

*Keywords:* Stewart platform; Hydraulic servomechanisms; Parallel mechanisms; Model-based control

---

## 1. Introduction

The original Gough six Degree-of-Freedom (dof) platform was developed in 1954 [1,2]. In 1965, the prototype parallel mechanism was used as a 6-dof motion platform for a flight simulator [3]. Since then, a number of studies on this mechanism and its variations have been published, i.e. [4]. The mechanism can be driven electrically or electrohydraulically. The kinematics and dynamics of the Stewart–Gough (S–G) platform has been studied by many researchers [5–9]. However, actuation dynamics have not been considered. Although electrohydraulic S–G platforms have been used extensively, little published work on their full dynamics including actuation and control, exists.

Hydraulics science combined with controls, has given new thrust to hydraulics applications. The main reasons why hydraulics are preferred to electromechanical drives in some industrial and mobile applications, include their ability to produce large forces at high speeds, their high durability and stiffness, and their rapid response [10]. Hydraulic regimes differ from electromechanical ones, in that the force or torque output is not

---

\* Corresponding author. Tel.: +30 210 772 1440; fax: +30 210 772 1455.  
E-mail address: [egpapado@central.ntua.gr](mailto:egpapado@central.ntua.gr) (E. Papadopoulos).

## Nomenclature

$A$	piston area [ $\text{m}^2$ ]
$b$	viscous friction parameter [ $\text{N s m}^{-1}$ ]
$C$	fluid capacitance [ $\text{m}^4 \text{s}^2 \text{kg}^{-1}$ ]
$C_d$	discharge coefficient [–]
$d_1, d_0$	system length parameter [m]
$\mathbf{e}$	position error vector
$f$	(a) servovalve nonlinear function [ $\text{m}^{7/2} \text{kg}^{-1/2}$ ], (b) excitation frequency [ $\text{s}^{-1}$ ]
$F_{\text{act}}$	actuator output force [N]
$\mathbf{F}_c, \mathbf{F}_v$	Coulomb, viscous friction vector
$F_c, F_s, F_v$	Coulomb, static and viscous friction force [N]
$F_{c0}, F_{s0}$	Coulomb and static friction parameter [N]
$F_{\text{ext}}$	external force [N]
$\mathbf{F}_{\text{fr}}, \mathbf{F}_{\text{fr}}^*$	friction vector
$F_{\text{fr},p}$	actuator friction force [N]
$\mathbf{F}_p$	actuator force vector
$F_p$	hydraulic piston force [N]
$\langle F \rangle$	vector element of $\mathbf{M}^* \ddot{\ell} + \mathbf{V}^* + \mathbf{G}^* + \mathbf{F}_{\text{fr}}^*$ [N]
$g$	(a) acceleration of gravity (a) [ $\text{m s}^{-2}$ ], (b) servovalve nonlinear function (b) [ $\text{m}^{7/2} \text{kg}^{-1/2}$ ]
$\mathbf{G}, \mathbf{G}^*$	gravity vector
$G_{p,\text{in}}$	internal leakage coefficient of cylinder [ $\text{m}^4 \text{s kg}^{-1}$ ]
$\mathbf{J}$	Jacobian matrix
$i$	servovalve current [A]
$I_{xx}, I_{yy}, I_{zz}$	moment of inertia about the center of platform mass of $X, Y, Z$ axis [ $\text{kg m}^2$ ]
$\mathbf{K}_p, \mathbf{K}_v$	control gain matrices
$K_{0,1}, K_1$	positive servovalve constants [ $\text{m}^{7/2} \text{kg}^{-1/2}$ ], [ $\text{m}^{7/2} \text{kg}^{-1/2}/\text{A}$ ]
$\ell$	actuator length [m]
$\ell$	actuator length vector
$m$	platform mass [kg]
$\mathbf{M}, \mathbf{M}^*$	mass matrix
$P$	total system power [W]
$p$	pressure [bar]
$p, q, r$	Euler angle of platform at $X, Y, Z$ axis [rad]
$p_c, q_c, r_c$	trajectory constants [rad]
$p_s, p_T$	power supply and return pressure [bar]
$Q$	fluid flow [ $\text{m}^3 \text{s}^{-1}$ ]
$r_0, r_1$	system length parameters [m]
$t$	time [s]
$\mathbf{V}, \mathbf{V}^*$	centrifugal and Coriolis vector
$\mathbf{x}$	generalized coordinates vector
$x_0, y_0, z_0$	generalized coordinates of the center of platform mass at $X, Y, Z$ axis [m]
$x_c, y_c, z_c, z_{c1}$	trajectory constants [m]
$\rho$	fluid mass density [ $\text{kg m}^{-3}$ ]
$\boldsymbol{\tau}$	torque/force vector
$\zeta$	close-loop natural damping [–]
$\omega$	close-loop natural frequency [rad/s]

*Indices*

act	actuator
C	Coulomb
des	desired
ext	external
fr	friction
in	internal
p	piston
s	(a) static, (b) supply
T	tank (return)
v	(a) valve, (b) viscous

proportional to actuator current and therefore, hydraulic actuators cannot be modelled as force/torque sources, but as controlled impedances. As a result, controllers that have been designed for robot control, assuming the capability of setting actuator force/ torque, cannot be used here.

Nguyen et al. [11] have developed a joint-space adaptive control scheme applied to an electromechanically driven Stewart platform-based manipulator, using the Lyapunov direct method, and under the assumption that platform motion is slow compared to the controller adaptation rate. Also, Kim and Lee studied and applied a high speed tracking control of a 6–6 electric Stewart platform, using an enhanced sliding mode control approach [12].

Control techniques can be used to compensate for the nonlinearities of electrohydraulic servosystems. Non-linear adaptive control techniques for hydraulic servosystems have been proposed by Garagic and Srinivasan assuming linearization [13], and by Sirouspour and Salcudean using backstepping [14], approaches. The modelling of an experimental hydraulic robot arm and the implementation of a model-based motion controller that compensates for dynamic forces have been presented by Honegger and Corke [15]. However, this controller was not successful partly due to the use of desired configuration information and not of the measured one. A tracking controller for electrohydraulic servosystems, but with force and pressure feedback requirements, has been developed, including a fast model-based force tracking loop [16].

Further, the modelling and control of an inverted, ceiling-mounted electrohydraulically driven Stewart platform has been studied, using the virtual work principle [17]. The controller employed pressure feedback. Work on the same mechanism, in which a Lyapunov analysis approach has been used for designing a nonlinear controller, has been presented in Ref. [18]. A robust tracking control design for a 6-dof hydraulically driven Stewart type mechanism has been developed, using two Lyapunov-based types of controllers [19].

In this paper, a model-based controller for a 6–6 electrohydraulic S–G platform with symmetric joint locations is developed. Dynamic models are used that describe the rigid body equations of the S–G platform and the hydraulics dynamics of its actuation system. Servovalve models and friction are included in the model. The developed control scheme employs rigid body and actuation dynamics and yields the servovalve input current vector, in analytical form, so that the error dynamics converge asymptotically to zero, independent of load variations. Unlike other approaches, in this one, feedback of force, pressure, acceleration or of their derivatives is not required. The performance of the developed controller is illustrated using typical trajectories. The proposed methodology can be extended to electrohydraulic serial or closed-chain manipulators and simulators.

## 2. Dynamic modelling

In this section, the dynamic model of a 6-dof electrohydraulic S–G platform servomechanism is developed. This is a six dof closed kinematic chain mechanism consisting of a fixed base and a movable platform with six electrohydraulic actuators supporting it, see Fig. 1.

The equations of motion of a S–G platform mechanism are derived using a Lagrangian formulation and are written as

$$\mathbf{M}(\mathbf{x})\ddot{\mathbf{x}} + \mathbf{V}(\mathbf{x}, \dot{\mathbf{x}}) + \mathbf{G}(\mathbf{x}) + \mathbf{F}_{fr}(\dot{\mathbf{x}}) = \boldsymbol{\tau} \quad (1)$$

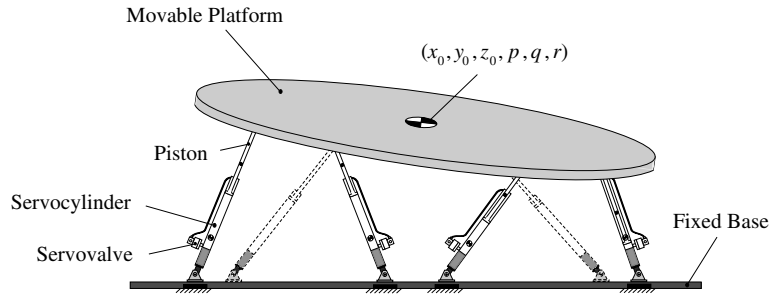


Fig. 1. Schematic view of a 6-dof S-G platform.

where  $\mathbf{x} = (x_0, y_0, z_0, p, q, r)^T$  is the  $6 \times 1$  vector of the platform generalized coordinates,  $x_0, y_0, z_0$ , are the platform center of mass Cartesian coordinates,  $p, q, r$  are the platform Euler angles,  $\mathbf{M}(\mathbf{x})$  is the  $6 \times 6$  positive definite mass matrix of the system, the  $6 \times 1$  vector  $\mathbf{V}(\mathbf{x}, \dot{\mathbf{x}})$  represents forces/torques arising from centrifugal and Coriolis forces, the  $6 \times 1$  vector  $\mathbf{G}(\mathbf{x})$  represents torques due to gravity,  $\mathbf{F}_{fr}(\dot{\mathbf{x}})$  is the  $6 \times 1$  vector of the forces/torques due to friction, and  $\boldsymbol{\tau}$  is the  $6 \times 1$  vector of the generalized applied forces.

Eq. (1) can be further extended using the transformation between mechanism actuator forces and the generalized applied forces [4], which is given by,

$$\boldsymbol{\tau} = \mathbf{J}^T \mathbf{F}_p \quad (2)$$

where  $\mathbf{J} = \mathbf{J}(\mathbf{x})$  is the Jacobian  $6 \times 6$  matrix of the system, and  $\mathbf{F}_p$  is a  $6 \times 1$  vector representing actuator forces given by,

$$\mathbf{F}_p = (F_{p,1}, F_{p,2}, \dots, F_{p,6})^T \quad (3)$$

where  $F_{p,j}, j = 1, 2, \dots, 6$  are individual hydraulic forces acting on the platform.

Further, using mechanism differential kinematics, see Appendix B, the platform Cartesian motion described by Eq. (1) can be transformed in its joint space and written as

$$\mathbf{M}^*(\mathbf{x})\ddot{\boldsymbol{\ell}} + \mathbf{V}^*(\mathbf{x}, \dot{\boldsymbol{\ell}}) + \mathbf{G}^*(\mathbf{x}) + \mathbf{F}_{fr}^*(\dot{\boldsymbol{\ell}}) = \mathbf{F}_p \quad (4)$$

where  $\boldsymbol{\ell} = (\ell_1, \ell_2, \dots, \ell_6)^T$  is the  $6 \times 1$  vector of the mechanism actuator lengths,  $\mathbf{M}^*(\mathbf{x})$  is a  $6 \times 6$  positive definite mass matrix, a  $6 \times 1$  vector  $\mathbf{V}^*(\mathbf{x}, \dot{\boldsymbol{\ell}})$  represents the centrifugal and Coriolis forces, the  $6 \times 1$  vector  $\mathbf{G}^*(\mathbf{x})$  represents the forces due to gravity, and  $\mathbf{F}_{fr}^*(\dot{\boldsymbol{\ell}})$  is the  $6 \times 1$  vector of the joint space friction forces. The terms  $\mathbf{M}^*(\mathbf{x})$ ,  $\mathbf{V}^*(\mathbf{x}, \dot{\boldsymbol{\ell}})$  and  $\mathbf{G}^*(\mathbf{x})$  are given, respectively by (see Appendix B),

$$\mathbf{M}^*(\mathbf{x}) = [\mathbf{J}(\mathbf{x})^T]^{-1} \mathbf{M}(\mathbf{x}) \mathbf{J}(\mathbf{x})^{-1} \quad (5a)$$

$$\mathbf{V}^*(\mathbf{x}, \dot{\boldsymbol{\ell}}) = [\mathbf{J}(\mathbf{x})^T]^{-1} [\mathbf{V}(\mathbf{x}, \dot{\mathbf{x}}) - \mathbf{M}(\mathbf{x}) \dot{\mathbf{J}}(\mathbf{x}, \dot{\mathbf{x}}) \cdot \dot{\mathbf{x}}] \quad (5b)$$

$$\mathbf{G}^*(\mathbf{x}) = [\mathbf{J}(\mathbf{x})^T]^{-1} \mathbf{G}(\mathbf{x}) \quad (5c)$$

A number of methods exists, that can be used to model the friction vector  $\mathbf{F}_{fr}^*(\dot{\boldsymbol{\ell}})$  [20]. A widely used method models friction as

$$\mathbf{F}_{fr}^*(\dot{\boldsymbol{\ell}}) = \mathbf{F}_v^*(\dot{\boldsymbol{\ell}}) + \mathbf{F}_c^*(\dot{\boldsymbol{\ell}}) + \mathbf{F}_s^* \quad (6)$$

where  $\mathbf{F}_v^*(\dot{\boldsymbol{\ell}})$ ,  $\mathbf{F}_c^*(\dot{\boldsymbol{\ell}})$  and  $\mathbf{F}_s^*$  are the viscous, Coulomb and static friction vector respectively, with elements,

$$F_{v,j}^*(\dot{\ell}_j) = \begin{cases} b_j \dot{\ell}_j, & \dot{\ell}_j \neq 0, \quad j = 1, 2, \dots, 6 \\ 0, & \dot{\ell}_j = 0, \quad j = 1, 2, \dots, 6 \end{cases} \quad (7a)$$

$$F_{c,j}^*(\dot{\ell}_j) = \begin{cases} F_{c0,j}^* \text{sign}(\dot{\ell}_j), & \dot{\ell}_j \neq 0, \quad j = 1, 2, \dots, 6 \\ 0, & \dot{\ell}_j = 0, \quad j = 1, 2, \dots, 6 \end{cases} \quad (7b)$$

$$F_{s,j}^* = \begin{cases} F_{ext,j}, & |F_{ext,j}| < F_{s0,j}^*, \dot{\ell}_j = 0, \ddot{\ell}_j = 0, \quad j = 1, 2, \dots, 6 \\ F_{s0,j}^* \text{sign}(F_{ext,j}), & |F_{ext,j}| > F_{s0,j}^*, \dot{\ell}_j = 0, \ddot{\ell}_j \neq 0, \quad j = 1, 2, \dots, 6 \\ 0, & \dot{\ell}_j \neq 0, \quad j = 1, 2, \dots, 6 \end{cases} \quad (7c)$$

where  $b_j$  is the  $j$ th parameter for viscous friction element,  $F_{c0,j}^*$  is the  $j$ th parameter for Coulomb friction element,  $F_{ext,j}$  is the  $j$ th external force element,  $F_{s0,j}^*$  is the  $j$ th breakaway force element and

$$\text{sign}(\dot{\ell}_j) = \begin{cases} +1, & \dot{\ell}_j > 0, \quad j = 1, 2, \dots, 6 \\ 0, & \dot{\ell}_j = 0, \quad j = 1, 2, \dots, 6 \\ -1, & \dot{\ell}_j < 0, \quad j = 1, 2, \dots, 6 \end{cases} \quad (8)$$

### 3. Hydraulic modelling

The electrohydraulic actuation servosystem of the platform consists of pistons, servovalves, controllers, sensors and a hydraulic power supply. Next, simple models of the system major components are introduced.

Hydraulic supplies include pumps that are usually constant pressure piston pumps, driven by induction electric motors. Therefore, a pump is modelled as a constant pressure source. Further, they may include accumulators for filtering pressure pulsations from the pump, but also for allowing the use of smaller rating pumps by providing additional flow when needed. Such an accumulator, is modelled as a hydraulic capacitor [21].

A single rod hydraulic servocylinder is illustrated schematically in Fig. 2. The equations relating mechanical to hydraulic variables are described by,

$$Q_1 = A_1 \dot{\ell} + C_1 \dot{p}_1 + G_{p,in}(p_1 - p_2) \quad (9a)$$

$$Q_2 = A_2 \dot{\ell} - C_2 \dot{p}_2 + G_{p,in}(p_1 - p_2) \quad (9b)$$

$$A_1 p_1 - A_2 p_2 = F_p \quad (9c)$$

$$F_{act} = F_p - F_{fr,p} \quad (9d)$$

where  $Q_1, Q_2$  are the flows through the two cylinder chamber ports,  $p_1, p_2$  are the chamber pressures,  $A_1$  is the piston side area,  $A_2$  is the rod side area,  $C_1, C_2$  are the fluid capacitances in the cylinder chambers,  $G_{p,in}$  represents the cylinder internal leakage conductance,  $F_p$  is the hydraulic force,  $F_{fr,p}$  is the actuator friction force, and  $F_{act}$  is the net actuator output force. In the case of a hydraulic cylinder with a double rod, the two areas  $A_1$  and  $A_2$  are equal and therefore, Eqs. (9) are simplified.

Control of a hydraulic system is achieved through the use of servovalves, see Fig. 3a. Only the resistive effect of a valve is considered here, since their natural frequency is much higher than that of the mechanical

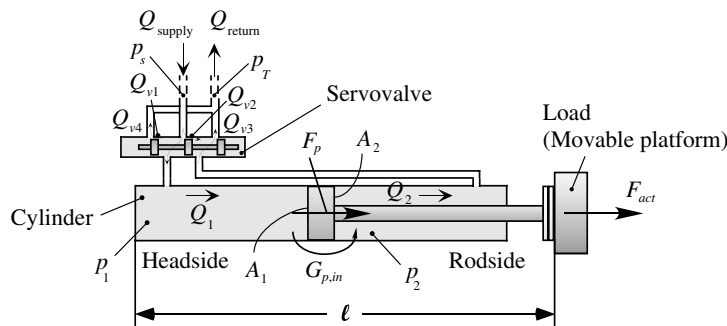


Fig. 2. Schematic model of hydraulic servoactuator.

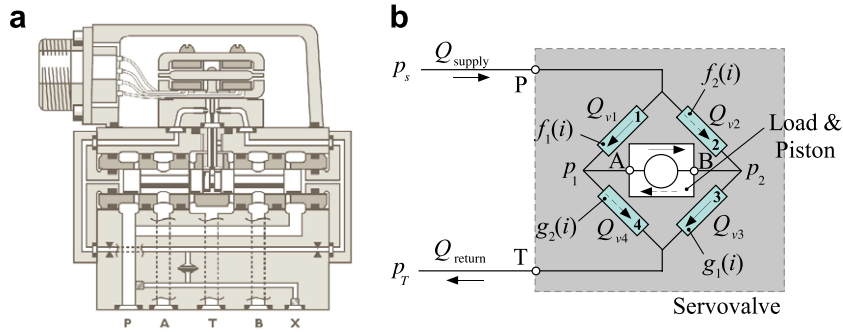


Fig. 3. (a) A drawing of a real servovalve, (b) schematic model of servovalve.

load. It is also assumed that the geometry of the valve is ideal, e.g. the valve has sharp edges and zero cross leakage [22,23].

A typical hydraulic servovalve consists of four symmetric and matched servovalve orifices making up flow paths through four nonlinear resistors, modulated by the input voltage, see Fig. 3a. Thereby, the servovalve is modelled as the hydraulic equivalent of a Wheatstone bridge, see Fig. 3b. When the servovalve input current is positive,  $i > 0$ , flow passes through the orifices 1 and 3 (path  $P - A - B - T$ ), and flow leakages exist in the valve orifices 2 and 4. Similarly, when the servovalve input current is negative,  $i < 0$ , flow passes through the path  $P - B - A - T$ , and flow leakages exist in the valve orifices 1 and 3. This model is described by,

$$Q_{v1} = f_1(i, C_d, \rho) \sqrt{p_s - p_1}, \quad Q_{v3} = g_1(i, C_d, \rho) \sqrt{p_2 - p_T} \quad (10a)$$

$$Q_{v2} = f_2(i, C_d, \rho) \sqrt{p_s - p_2}, \quad Q_{v4} = g_2(i, C_d, \rho) \sqrt{p_1 - p_T} \quad (10b)$$

where  $Q_{v1}$ ,  $Q_{v2}$ ,  $Q_{v3}$  and  $Q_{v4}$  are the servovalve flows through the orifices 1, 2, 3 and 4 respectively,  $p_s$  and  $p_T$  are the power supply and return pressure of the servosystem, correspondingly,  $i$  is the servovalve motor current (control command), and  $f_1(i, C_d, \rho)$ ,  $f_2(i, C_d, \rho)$ ,  $g_1(i, C_d, \rho)$  and  $g_2(i, C_d, \rho)$  are nonlinear functions in the servovalve motor current, the discharge coefficient  $C_d$  and the mass density of the fluid,  $\rho$ . In general, the discharge coefficient is as function of the *Reynolds* number and valve geometry. However, fluid density and Reynolds dependencies are weak for turbulent flow and therefore only the current dependency is significant here [10]; therefore, the functions  $f_1(i, C_d, \rho)$ ,  $f_2(i, C_d, \rho)$ ,  $g_1(i, C_d, \rho)$  and  $g_2(i, C_d, \rho)$  are reduced to  $f_1(i)$ ,  $f_2(i)$ ,  $g_1(i)$  and  $g_2(i)$ , correspondingly. Because of servovalve symmetry, the current functions are given by,

$$f_1(i) = g_1(i) = f_2(-i) = g_2(-i) \quad (11a)$$

$$f_2(i) = g_2(i) = f_1(-i) = g_1(-i) \quad (11b)$$

Experimental results showed that it is a good approximation to assume that these functions are linear functions of the input current, when flow passes through the main path, and have a constant value when flow passes through the leakage flow path. For instance, when  $i > 0$ , the main flow path passes through the orifices 1 and 3 and therefore the functions of Eqs. (10) are written as

$$f_1(i) = g_1(i) = K_1 i + K_{0,1} \quad (12a)$$

$$f_2(i) = g_2(i) = K_{0,1} \quad (12b)$$

where  $K_1$  and  $K_{0,1}$  are positive constants, which correspond to the main and leakage valve flow paths.

The  $K_1$  and  $K_{0,1}$  constants for a two-land-four-way spool MOOG servovalve were experimentally computed [16], and the results are depicted in Fig. 4.

If leakage flows and cylinder chamber compressibility are neglected, the flows through the orifices of the servovalve described by Eqs. (9a), (9b) are equal to the flows through cylinder chamber ports, see Eqs. (9a), (9b), and are written as

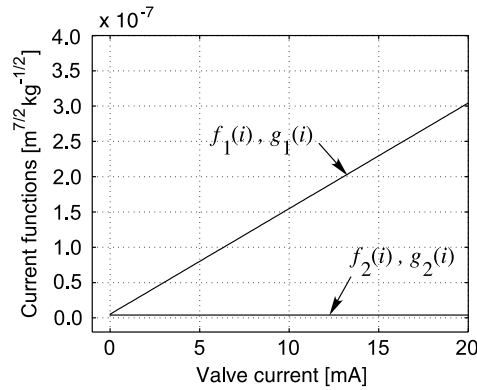


Fig. 4. Servo valve current functions in main and leakage path.

$$Q_{v1} = Q_1 = A_1 \dot{\ell} \quad (13a)$$

$$Q_{v3} = Q_2 = A_2 \dot{\ell} \quad (13b)$$

## 4. Control design

### 4.1. Feedback control scheme

In this section, candidate control schemes are studied and evaluated for implementation in a real-time environment. The schemes are discussed in terms of building blocks, computational burden, and feedback required to achieve tracking control of the platform; the low-level control design is developed in later sections. Three such concepts of control schemes are presented and discussed next.

The first control scheme, see Fig. 5a, called here an Operational Space control scheme, (OS), uses a feedback of the Cartesian coordinates of the platform. The controller uses the error in Cartesian coordinates to compute the system control input, i.e. the valve currents. The second control scheme, see Fig. 5b, called here a Joint Space (JS) control scheme, uses mechanism inverse kinematics for computing desired actuator length trajectories from desired Cartesian trajectories. The actuator error lengths and speeds are fed into the controller. In this scheme, actuator length feedback, provided by built-in sensors, is used. The third scheme, called here called an Operational Error Joint Feedback (OEJF) control scheme, embeds the forward kinematics in the feedback control loop, see Fig. 5c. Here, the computed Cartesian coordinate feedback is compared to the desired Cartesian trajectories to yield the trajectory error driving the controller.

Examining the three alternative control schemes, we observe that the first, OS, appears to be preferable, since it closes the loop on the actual platform position and orientation. However, this scheme requires Cartesian position and orientation sensors, which may be very expensive or impossible to find at the desired accuracies. The JS and OEJF schemes are advantageous from the practical point of view, since they require leg displacement sensors that are present in all such mechanisms. On the other hand, these schemes present some algorithmic complexities and numerical difficulties due to the use of forward kinematics that are described by complex nonlinear equations, and can be solved numerically only.

This characteristic is undesirable from the point of view of real-time control implementation, and cannot be bypassed. Fortunately, today's embedded computers can solve the forward kinematics in 5–15 ms, making it possible to implement controllers such as JS and OEJF in real-time. If additional bandwidth is needed, the computation time can be further reduced by using additional auxiliary linear or rotary sensors that are inexpensive and easy to add [24,25]. Using these techniques, additional joint positions of the mechanism are measured and the forward kinematics equations can be written as a linear algebraic system constrained by the proper orthogonality of the rotation matrix. Usually, in S–G systems, joint angular sensors are preferred to additional displacement sensors (due to implementation difficulties, link collision avoidance, etc.).

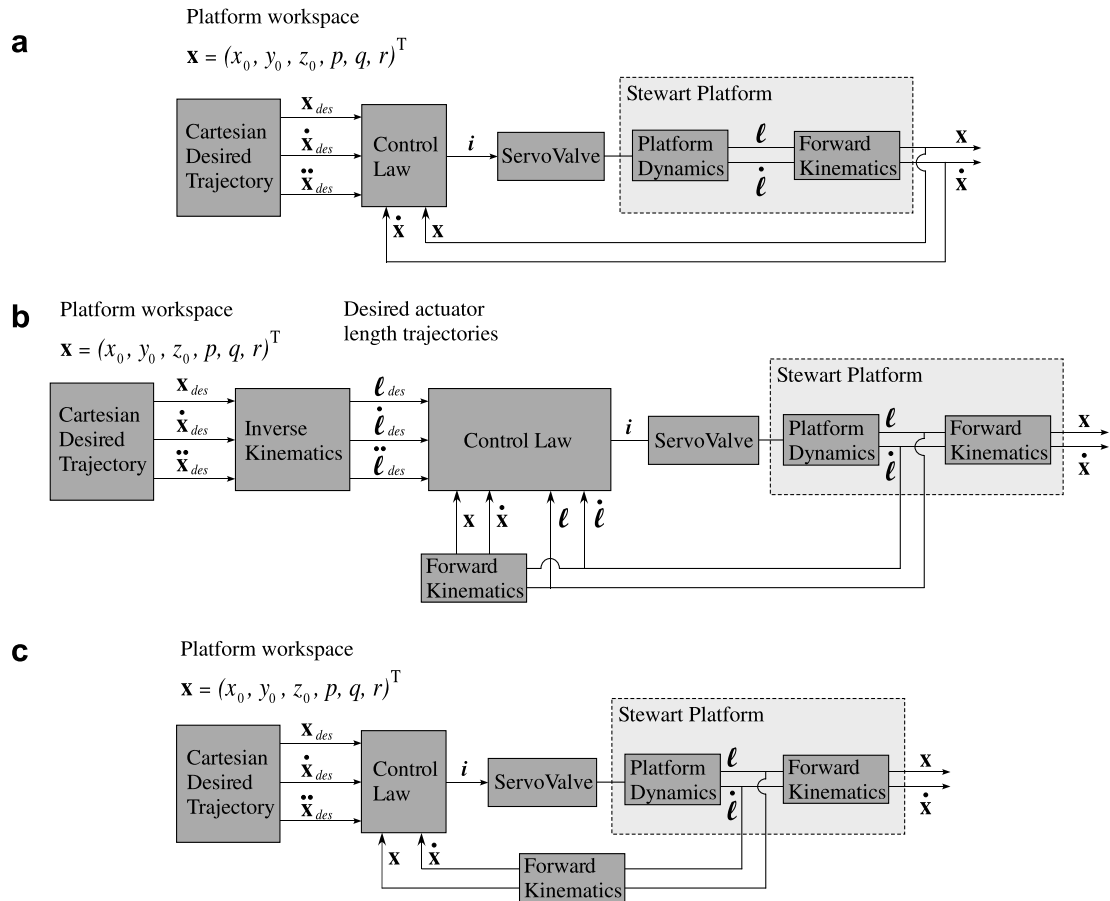


Fig. 5. Alternatives model-based control schemes: (a) OS controller, (b) JS controller, and (c) OEJF controller.

We note here that all control schemes in Fig. 5 depend on the knowledge of system parameters. Errors in system parameters may result in deviation of the platform position and orientation from those desired. This problem can be solved using appropriate identification procedures and calibration techniques [26,27].

As mentioned earlier, JS and OEJF are advantageous from the feedback point of view. Comparing these two, we observe that JS requires additional computations due to the use of inverse kinematics. Therefore, OEJF is preferable and is selected for further implementation of the model-based controller.

#### 4.2. Model-based controller

In this section, the selected OEJF control scheme is used to develop a novel model-based controller allowing tracking of the reference inputs for the six-dof electrohydraulic S–G platform. Desired Cartesian trajectories are used as input commands of the controller. The control law provides the current sent to the linear hydraulic servoactuator servovalves. The control analysis is based on the system dynamic and hydraulic model; therefore, it is assumed that the dynamic terms  $\mathbf{M}(\mathbf{x})$ ,  $\mathbf{V}(\mathbf{x}, \dot{\mathbf{x}})$ ,  $\mathbf{G}(\mathbf{x})$ , and  $\mathbf{F}_{fr}(\dot{\mathbf{x}})$  see Eq. (1), are known. This usually requires some identification experiments, see for example [16].

In the electromechanical domain, actuator Lorentz forces are proportional to actuator current. This simplifies motion control laws and allows one to achieve second-order error dynamics converging exponentially to zero. However, a simple relationship between force and current does not exist in electrohydraulic systems. Despite this, we are interested in studying whether such a system can be described by decoupled invariant error dynamics, so that the error dynamics converge asymptotically to zero, independent of load variations. The

error dynamics equation which describe such a requirement is given by a second-order differential equation such as

$$\ddot{\mathbf{e}} + \mathbf{K}_v \dot{\mathbf{e}} + \mathbf{K}_p \mathbf{e} = \mathbf{0} \quad (14)$$

where  $\mathbf{K}_p$ ,  $\mathbf{K}_v$  are  $6 \times 6$  diagonal matrices, which represent the control gains of the system, and  $\mathbf{e}$  is the  $6 \times 1$  position error vector of the moving platform, given by,

$$\mathbf{e} = \mathbf{x}_{\text{des}} - \mathbf{x} \quad (15)$$

where  $\mathbf{x}_{\text{des}}$  is the  $6 \times 1$  vector of the desired platform displacements. Note that the error dynamics in (14) are independent of the system inertial properties, i.e. tracking error transient and convergence do not depend on load variations.

Since Eq. (14) is a second-order differential equation, matrix factors  $\mathbf{K}_p$  and  $\mathbf{K}_v$  can be written in terms of the closed-loop natural frequency and damping,  $\omega_j$  and  $\zeta_j$ ,  $j = 1, 2, \dots, 6$ , respectively, for the six linear actuators. Therefore, these are given by,

$$\mathbf{K}_p = \text{diag}\{\omega_1^2, \omega_2^2, \dots, \omega_6^2\} \quad (16a)$$

$$\mathbf{K}_v = \text{diag}\{2\zeta_1\omega_1, 2\zeta_2\omega_2, \dots, 2\zeta_6\omega_6\} \quad (16b)$$

The  $\omega_j$  and  $\zeta_j$ ,  $j = 1, 2, \dots, 6$ , determine the system's stability and affect critically its transient response. Therefore, the closed-loop natural frequency and damping are selected so that the closed-loop poles lie in a desirable area of the left half complex plane.

Using Eqs. (9), (12) and (13), the servocylinder chamber pressures are computed as

$$p_1|_j = \left[ p_s - \frac{A_1^2}{(K_1 i + K_{0,1})^2} \cdot \dot{\ell}^2 \right]_j, \quad j = 1, 2, \dots, 6 \quad (17a)$$

$$p_2|_j = \left[ p_T + \frac{A_2^2}{(K_1 i + K_{0,1})^2} \cdot \dot{\ell}^2 \right]_j, \quad j = 1, 2, \dots, 6 \quad (17b)$$

Using Eqs. (9c) and (17), the hydraulic forces developed by the actuators are given by,

$$[p_1 A_1 - p_2 A_2]|_j = \left[ A_1 p_s - A_2 p_T - \frac{A_1^3 + A_2^3}{(K_1 i + K_{0,1})^2} \cdot \dot{\ell}^2 \right]_j, \quad j = 1, 2, \dots, 6 \quad (18)$$

where  $i_j$  is the current (control input) for the  $j$ th valve/actuator assembly and  $[p_1 A_1 - p_2 A_2]|_j$  is the resulting actuator force. However, Eq. (18) is also function of the velocity of the actuators,  $\dot{\ell}_j$ . Substituting Eq. (18) in the system equation of motion, Eq. (1), the following equations of motion are derived,

$$\{[\mathbf{J}(\mathbf{x})^T]^{-1} \cdot [\mathbf{M}(\mathbf{x})\ddot{\mathbf{x}} + \mathbf{V}(\mathbf{x}, \dot{\mathbf{x}}) + \mathbf{G}(\mathbf{x}) + \mathbf{F}_{fr}(\dot{\mathbf{x}})]\} = \begin{bmatrix} \left[ A_1 p_s - A_2 p_T - \frac{A_1^3 + A_2^3}{(K_1 i + K_{0,1})^2} \cdot \dot{\ell}^2 \right]_1 \\ \vdots \\ \left[ A_1 p_s - A_2 p_T - \frac{A_1^3 + A_2^3}{(K_1 i + K_{0,1})^2} \cdot \dot{\ell}^2 \right]_6 \end{bmatrix} \quad (19)$$

Solving Eq. (19) for the input commands,  $i_j$ ,  $j = 1, 2, \dots, 6$ , the components of the servovalve current vector  $\mathbf{i} = (i_1, i_2, \dots, i_6)^T$  are computed as

$$i_j = \left[ \frac{\dot{\ell}}{K_1 \sqrt{\frac{1}{A_1^3 + A_2^3}} [A_1 p_s - A_2 p_T - \langle F \rangle]} - \frac{K_{0,1}}{K_1} \right]_j, \quad j = 1, 2, \dots, 6 \quad (20)$$

where  $\langle F \rangle|_j$  represents the  $j$ th element of the vector  $[\mathbf{J}(\mathbf{x})^T]^{-1} \cdot [\mathbf{M}(\mathbf{x})\ddot{\mathbf{x}} + \mathbf{V}(\mathbf{x}, \dot{\mathbf{x}}) + \mathbf{G}(\mathbf{x}) + \mathbf{F}_{fr}(\dot{\mathbf{x}})]$ .

Further, assuming that Eq. (14) has been achieved, Eq. (7b) is solved for  $\ddot{\mathbf{x}}$  and the result is substituted in the elements  $\langle F \rangle_j$ . Then, the  $\langle F \rangle_j$  are given by,

$$\langle F \rangle_j = \{ [\mathbf{J}(\mathbf{x})^T]^{-1} \cdot [\mathbf{M}(\mathbf{x}) \cdot (\ddot{\mathbf{x}}_{des} + \mathbf{K}_v \dot{\mathbf{e}} + \mathbf{K}_p \mathbf{e}) + V(\mathbf{x}, \dot{\mathbf{x}}) + \mathbf{G}(\mathbf{x}) + \mathbf{F}_{fr}(\dot{\mathbf{x}})] \}_j, \quad j = 1, 2, \dots, 6 \quad (21)$$

Eqs. (20), (21) correspond to a model-based closed-loop controller that yields the servovalve current vector for a given desired trajectory. The controller includes a model of both the mechanism and the electrohydraulic actuation dynamics. In Eq. (21), it is assumed that  $\mathbf{J}(\mathbf{x})^T$  can be inverted anywhere, with the exception of mechanism singular configurations. However, such a platform will never be driven through singular configurations, as this is checked by a separate code that does not allow the mechanism to pass through such dangerous poses.

The developed controller, given by Eqs. (20), (21), requires feedback of cylinder position and cylinder velocity errors only. As can be seen from Eq. (20), the servovalve current inputs are functions of the position and velocity error vector, i.e.,

$$\mathbf{i} = \mathbf{i}(\mathbf{e}, \dot{\mathbf{e}}) \quad (22)$$

The controller also uses the *desired* acceleration, i.e. no acceleration measurement is required. In contrast to other approaches, here, force, pressure or acceleration feedback or their derivatives are not required. These variables are typically difficult to obtain, require additional sensing and are contaminated with noise. The fact that this controller does not require feedback of these is a clear advantage when it comes to implementing it. The block diagram in Fig. 5c indicates the position of this controller in the overall system, in which it is represented by the block labeled “control law.”

Substituting Eq. (20) in Eqs. (10), and combining Eqs. (1), (2), (9) and (13), an equation of the form of Eq. (14) results, which demonstrates the stability of the system. The response is stable provided that the gain matrices are nonnegative while the error transient depends on the particular gain selection.

## 5. Simulation results

The tracking performance of the controller is evaluated next. Usually, in flight simulators, the platform mass is much larger than the mass of the actuators. Due to this fact, and to simplify the terms in the equations of motion for the needs of this paper, the terms  $\mathbf{M}(\mathbf{x})$ ,  $\mathbf{V}(\mathbf{x}, \dot{\mathbf{x}})$  and  $\mathbf{G}(\mathbf{x})$  of Eq. (1) are simplified by neglecting actuator masses. The resulting matrices and vectors, i.e.,  $\mathbf{M}(\mathbf{x})$ ,  $\mathbf{V}(\mathbf{x}, \dot{\mathbf{x}})$  and  $\mathbf{G}(\mathbf{x})$  are given in Appendix A, see Eqs. (A1)–(A3). Here, the system parameters include the platform mass  $m = 300$  kg, the moments of inertia about the platform center of mass  $I_{xx} = I_{yy} = 25$  kg m<sup>2</sup>,  $I_{zz} = 50$  kg m<sup>2</sup>, and friction parameters,  $b_j$ ,  $F_{c0,j}^*$  and  $F_{s0,j}^*$ . Friction parameters were experimentally computed using a single electrohydraulic actuator, in a configuration similar to that of a S–G platform [16]. The identification experiments results are shown in Fig. 6. These yield,  $b_j = 760$  N s/m,  $F_{c0,j}^* = 71$  N and  $F_{s0,j}^* = 245$  N during piston expansion, and  $b_j = 945.59$  N s/m,  $F_{c0,j}^* = -16.5$  N and  $F_{s0,j}^* = -210$  N during piston compression. Mechanical parametric uncertainties can be neglected here, as the controller performance is not sensitive to these. However, an uncertainty analysis is presented in [28]. A top view of a 6–6 symmetric S–G mechanism is illustrated in Fig. 7. The joints of the movable platform and fixed base lie at equal peripheral distances and at radii  $r_1 = 0.5$  m and  $r_0 = 1.0$  m, respectively; the joint distances at the movable platform and fixed base are  $d_1 = 0.2$  m and  $d_0 = 0.3$  m, respectively, see Fig. 7. Further, the valve parameters are  $K_{0,1} = 5.13 \times 10^{-9}$  (m<sup>7</sup>/kg)<sup>1/2</sup> and  $K_1 = 1.50 \times 10^{-5}$  m<sup>7/2</sup>/(A kg<sup>1/2</sup>), see Fig. 4.

The Cartesian desired trajectories of the platform center of mass are assumed to be

$$x_0(t) = x_c \sin(2\pi f_1 t), \quad y_0(t) = y_c \cos(2\pi f_1 t), \quad z_0(t) = z_{c1} + z_c \sin(2\pi f_1 t) \quad (23a)$$

$$p(t) = p_c \cos(2\pi f_2 t), \quad q(t) = q_c \sin(2\pi f_2 t), \quad r(t) = r_c \sin(2\pi f_2 t) \quad (23b)$$

where  $x_c$ ,  $y_c$ ,  $z_c$ ,  $z_{c1}$ ,  $p_c$ ,  $q_c$  and  $r_c$  are trajectory constants,  $f_1$ ,  $f_2$  are the corresponding position and orientation platform trajectory frequencies, and  $t$  is the time. The trajectory parameters are,  $f_1 = 0.6$  Hz,  $f_2 = 0.3$  Hz,  $x_c = 0.2$  m,  $y_c = 0.1$  m,  $z_c = 0.1$  m,  $z_{c1} = 1.26$  m,  $p_c = 10^\circ$ ,  $q_c = 30^\circ$ ,  $r_c = 30^\circ$ . To compute the matrix control gains, we first require that the response of all dofs is critically damped. Hence,  $\zeta_j = 1$ ,  $j = 1, 2, \dots, 6$ . Next,

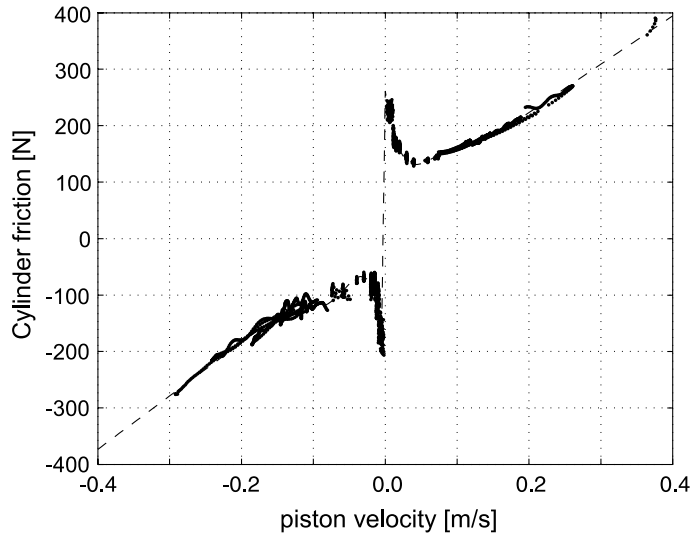


Fig. 6. Experimental results of a hydraulic cylinder friction force vs. piston velocity [16].

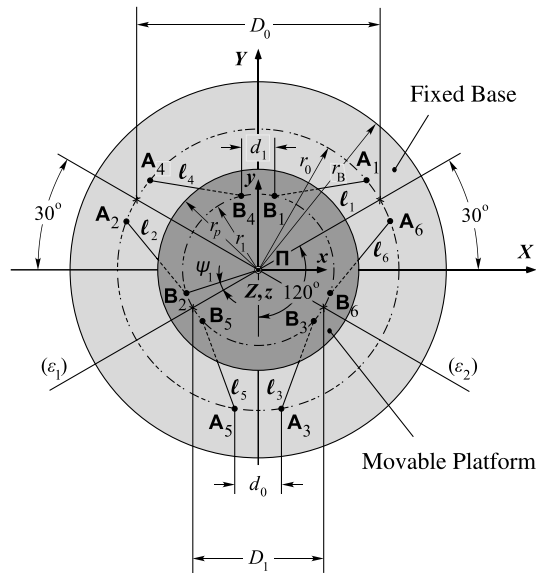


Fig. 7. Ground plan of a six-dof S-G platform.

to keep power requirements under control, we require a settling time of about  $t_s = 0.2$  s, yielding  $\omega_j = 10\pi$  rad/s,  $j = 1, 2, \dots, 6$ . Eq. (16) yield then the elements of  $\mathbf{K}_p$  and  $\mathbf{K}_v$  matrices,  $K_{p,j} = 100\pi^2$  rad<sup>2</sup>/s<sup>2</sup> and  $K_{v,j} = 20\pi$  rad/s,  $j = 1, 2, \dots, 6$ .

Figs. 7 and 8 show the response to the desired trajectories given by Eqs. (23). The platform displacements in the three Cartesian axes and orientation are shown in Fig. 8, and the position and orientation errors of the platform are depicted in Fig. 9. The position errors converge to zero, as expected, and the settling time is  $t_{s,j} = 6/\omega_j$ [s],  $j = 1, 2, \dots, 6$ . Also, the position response of one of the six leg lengths of the mechanism, the force acting on the platform, the input signal for the same actuator, and the total power of the system are depicted in Fig. 10.

The robustness of the controller can be demonstrated by applying the controller to the system in the case of erroneous parameter estimation. For example, assume that the platform load is estimated to be 5% larger than

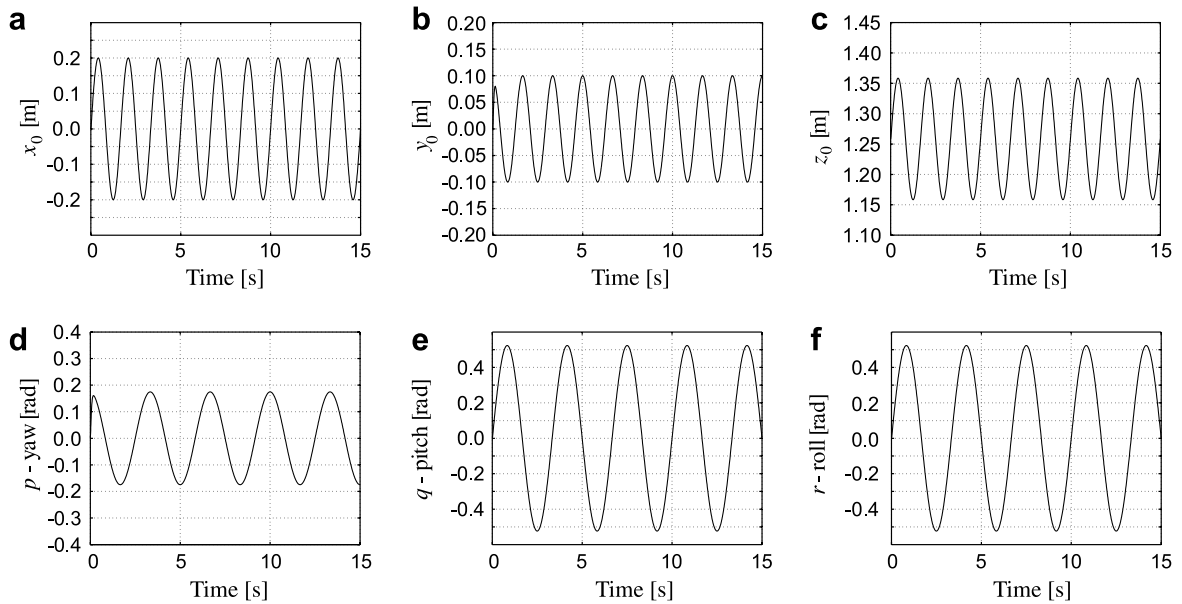


Fig. 8. Simulation results. (a–c) Platform displacement response, (d–f) platform orientation.

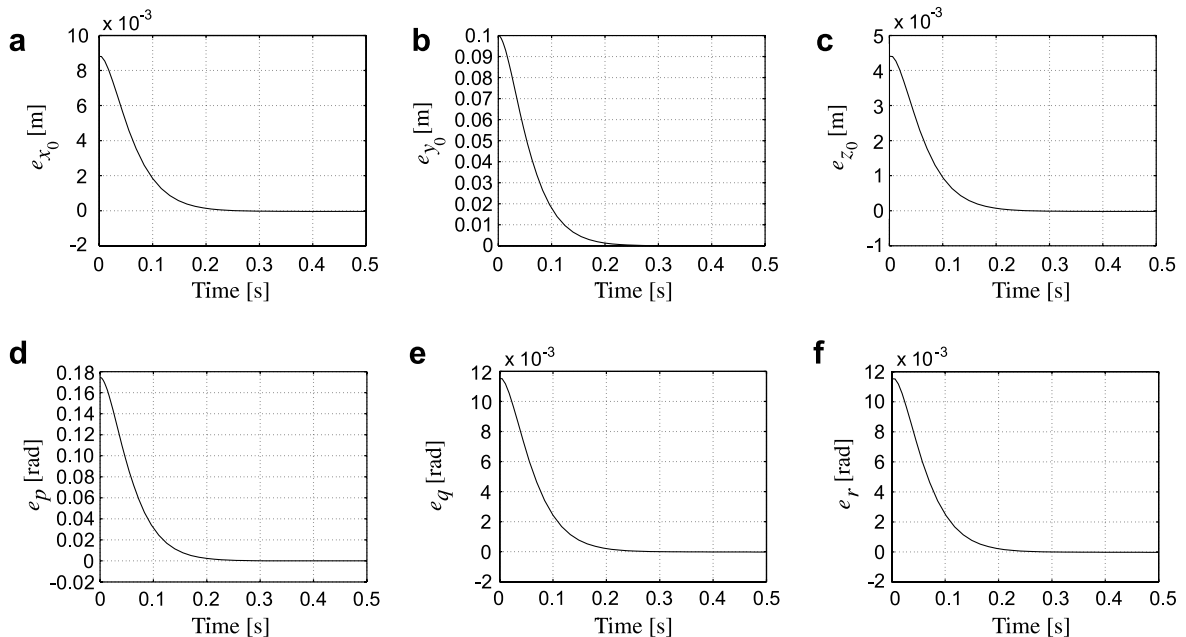


Fig. 9. Simulation results. (a–c) Platform position errors, (d–f) platform orientation errors.

its true value and all joint locations for both the movable platform and fixed base differ by 5% from their true values. These are rather strong assumptions, especially for the kinematic errors, as such platforms are designed at high tolerances for ensuring smoothness of operation. The new platform position and orientation errors are illustrated in Fig. 11. The comparison between Figs. 8 and 11 demonstrates that despite the introduction system parameter inaccuracies, the controller leads the system to the desired location, with a small increase of platform position and orientation errors.

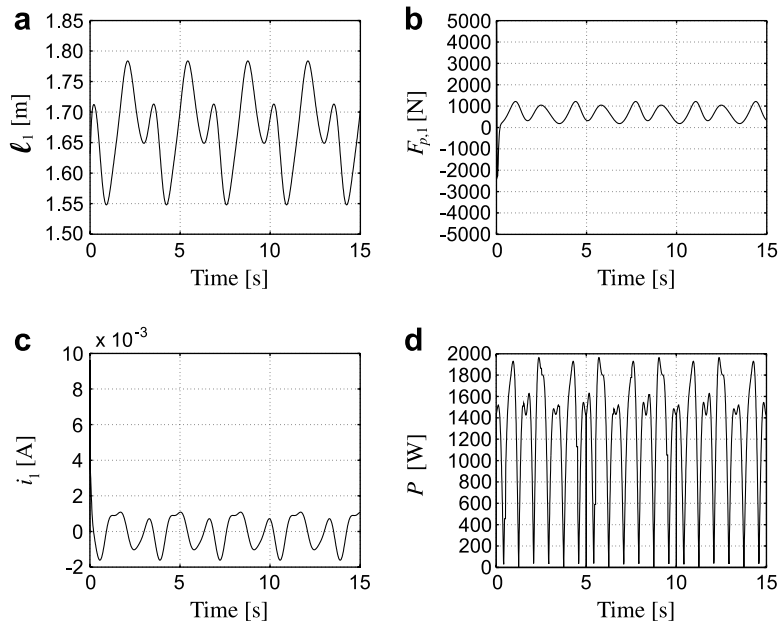


Fig. 10. Simulation results. A servoactuator: (a) length position, (b) actuated force, (c) input signal, and (d) total system power.

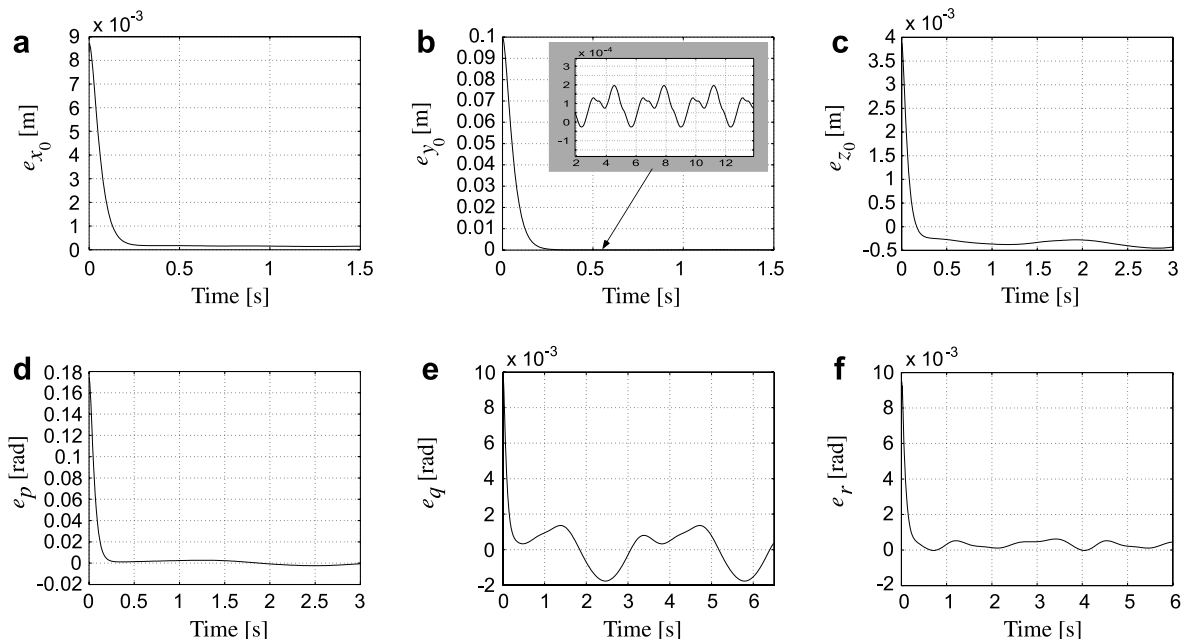


Fig. 11. Simulation results with a parametric error of  $\pm 5\%$ . (a–c) Platform position errors, (d–f) platform orientation errors.

The above examples showed that a model-based controller can be developed for an electrohydraulic system, despite the intrinsic nature of the system, which is very different from electrically driven robots. Uncertainty always exists, but the proposed controller works even in the presence of relatively large parametric uncertainty. Obviously, a better knowledge of the parameters improves the response, and this is to be expected. Reducing parameter uncertainty beyond some threshold requires either the use of a parameter identification method or of an adaptive controller.

## 6. Conclusions

The development of a novel model-based control for a 6–6 electrohydraulic Stewart–Gough platform was studied. Rigid body equations describing the S–G platform motion and its hydraulic dynamics, including friction and servovalve models were employed. The feedback controller approach used the system dynamic and hydraulic model to yield servovalve currents, so that the error dynamics converge asymptotically to zero, independent of the applied load. In this approach, force, pressure or acceleration feedback was not required. Simulations with typical desired trajectory inputs were presented and a satisfactory performance of the controller was observed. The proposed methodology can be extended to electrohydraulic serial or closed-chain manipulators and simulators.

## Acknowledgements

Support by the EPAN Cooperation Program 4.3.6.1 (Greece-Poland) of the Hellenic General Secretariat for Research and Technology and the NTUA Senator Committee of Basic Research Programme “Protogoras”, R.C. No. 10, is acknowledged.

## Appendix A.

The  $6 \times 6$  mass matrix of the platform,  $\mathbf{M}$ , and  $6 \times 1$  vectors  $\mathbf{V}$  and  $\mathbf{G}$  of the Stewart mechanism, in case that the dynamics of mechanism actuators is neglected, are given by,

$$\mathbf{M} = \begin{pmatrix} m & 0 & 0 & 0 & 0 & 0 \\ 0 & m & 0 & 0 & 0 & 0 \\ 0 & 0 & m & 0 & 0 & 0 \\ 0 & 0 & 0 & M(4,4) & M(4,5) & I_{zz} \cos q \\ 0 & 0 & 0 & M(5,4) & M(5,5) & 0 \\ 0 & 0 & 0 & I_{zz} \cos q & 0 & I_{zz} \end{pmatrix} \quad (\text{A.1a})$$

$$\mathbf{V} = (0, 0, 0, V(4,1), V(5,1), V(6,1))^T \quad (\text{A.1b})$$

$$\mathbf{G} = (0, 0, 0, mg, 0, 0)^T \quad (\text{A.1c})$$

where,

$$M(4,5) = M(5,4) = \frac{1}{2}(I_{yy} - I_{xx}) \cdot \sin q \cdot \sin 2r \quad (\text{A.2a})$$

$$M(4,4) = \frac{1}{4}[I_{xx} + I_{yy} + 2I_{zz} - (I_{xx} + I_{yy} - 2I_{zz}) \cdot \cos 2q + 2 \cdot (I_{xx} - I_{yy}) \cdot \cos 2r \cdot \sin^2 q] \quad (\text{A.2b})$$

$$M(5,5) = \frac{1}{2}[I_{xx} + I_{yy} + (I_{yy} - I_{xx}) \cdot \sin 2r] \quad (\text{A.2c})$$

and,

$$\begin{aligned} V(4,1) = & \frac{1}{2}\{(I_{yy} - I_{xx})\dot{q}^2 \cos q \cdot \sin 2r - 2I_{zz}\dot{q}\dot{r} \sin q - 2(I_{xx} - I_{yy}) \cdot \\ & \dot{q}\dot{r} \sin q \cdot \cos 2r + [I_{xx} + I_{yy} - 2I_{zz} + (I_{xx} - I_{yy}) \cos 2r] \cdot \\ & \dot{p}\dot{q} \sin 2q + (I_{yy} - I_{xx})\dot{p}\dot{q}\dot{r} \sin^2 q \cdot \sin 2r\} \end{aligned} \quad (\text{A.3a})$$

$$\begin{aligned} V(5,1) = & \frac{1}{4}\{[2I_{zz} - I_{xx} - I_{yy} - (I_{xx} - I_{yy}) \cos 2r]\dot{p}^2 \cos 2q \\ & + 4[I_{zz} + (I_{yy} - I_{xx}) \cos 2r]\dot{p}\dot{r} \sin q + 4(I_{xx} - I_{yy})\dot{q}\dot{r} \sin 2r\} \end{aligned} \quad (\text{A.3b})$$

$$V(6,1) = \frac{1}{2}\{(I_{xx} - I_{yy})\dot{p}^2 \sin^2 q \cdot \sin 2r - 2[I_{zz} + (I_{yy} - I_{xx}) \cdot \cos 2r]\dot{p}\dot{q} \sin q - (I_{xx} - I_{yy})\dot{q}^2 \sin 2r\} \quad (\text{A.3c})$$

## Appendix B.

The  $6 \times 6$  Jacobian matrix,  $\mathbf{J}(\mathbf{x})$ , combines the generalized velocities,  $\dot{\mathbf{x}}$ , with the actuator velocities,  $\dot{\ell} = (\dot{\ell}_1, \dot{\ell}_2, \dots, \dot{\ell}_6)^\top$  via the relationship,

$$\dot{\ell} = \mathbf{J}(\mathbf{x}) \cdot \dot{\mathbf{x}} \quad (\text{B.1})$$

This equation leads to,

$$\dot{\mathbf{x}} = [\mathbf{J}(\mathbf{x})]^{-1} \cdot \dot{\ell} \quad (\text{B.2a})$$

$$\ddot{\mathbf{x}} = [\mathbf{J}(\mathbf{x})]^{-1} \cdot \ddot{\ell} - [\mathbf{J}(\mathbf{x})]^{-1} \dot{\mathbf{J}}(\mathbf{x}, \dot{\mathbf{x}}) \cdot \dot{\mathbf{x}} \quad (\text{B.2b})$$

Finally, substitution of Eq. (B.2b) in Eq. (1), yields Eq. (4).

## Appendix C

The actuator lengths are determined using inverse kinematics of the mechanism. Given the generalized coordinates,  $\mathbf{x} = (x_0, y_0, z_0, p, q, r)^\top$ , the actuator lengths are expressed by,

$$\begin{aligned} \ell_i = \{ & x_{B_i}^2 + y_{B_i}^2 + z_{B_i}^2 + (X_{A_i} - x_0)^2 + (Y_{A_i} - y_0)^2 + (Z_{A_i} - z_0)^2 - 2[(r_{11}x_{B_i} + r_{12}y_{B_i} + r_{13}z_{B_i}) \cdot (X_{A_i} - x_0) \\ & + (r_{21}x_{B_i} + r_{22}y_{B_i} + r_{23}z_{B_i}) \cdot (Y_{A_i} - y_0) + (r_{31}x_{B_i} + r_{32}y_{B_i} + r_{33}z_{B_i}) \cdot (Z_{A_i} - z_0)]\}^{1/2}, \quad i = 1, 2, \dots, 6 \end{aligned} \quad (\text{C.1})$$

where  $X_{A_i}, Y_{A_i}, Z_{A_i}$  are the coordinates of joints  $A_i$  relative to  $XYZ$  frame, see Fig. 7,  $x_{B_i}, y_{B_i}, z_{B_i}$  are the coordinates of joints  $B_i$  relative to  $xyz$  frame, see Fig. 7, and  $r_{11}, r_{12}, \dots, r_{33}$  are the elements of rotation matrix of the platform, which are given by,

$$r_{11} = \cos p \cos q \cos r - \sin p \sin r, \quad r_{12} = -\cos r \sin p - \cos p \cos q \sin r, \quad r_{13} = \cos p \sin q \quad (\text{C.2a})$$

$$r_{21} = \cos q \cos r \sin p + \cos p \sin r, \quad r_{22} = \cos p \cos r - \cos q \sin p \sin r, \quad r_{23} = \sin p \sin q \quad (\text{C.2b})$$

$$r_{31} = -\cos \gamma \sin q, \quad r_{32} = \sin q \sin r, \quad r_{33} = \cos q \quad (\text{C.2c})$$

## References

- [1] V.E. Gough, Discussion in London: automobile stability, control, and tyre performance, in: Proceedings of the IMechE's Automobile Division, 1956, pp. 392–394.
- [2] The true origins of parallel Robots, <<http://www.parallelemic.org>>.
- [3] D. Stewart, A platform with six degrees of freedom, in: Proceedings of the IMechE, vol. 180, Pt. 1, No. 15, 1965–1966, pp. 371–385.
- [4] L.W. Tsai, Robot Analysis, The Mechanics of Serial and Parallel Manipulators, Springer, 1999.
- [5] J.H. Shim, J.Y. Park, D.S. Kwon, S. Kim, Kinematic, design of a six degree-of-freedom in-parallel manipulator for probing task, in: Proceedings of the IEEE International Conference on Robotics and Automation, New Mexico, 1997, pp. 2967–2973.
- [6] M.J. Liu, C.X. Li, C.N. Li, Generalized Stewart–Gough platforms and their direct kinematics, IEEE Transactions on Robotics and Automation 16 (1) (2000) 94–98.
- [7] X.S. Gao, D. Lei, Q. Liao, G.F. Zhang, Generalized Stewart–Gough platforms and their direct kinematics, IEEE Transactions on Robotics 21 (2) (2005) 141–151.
- [8] G. Leuret, K. Liu, F.L. Lewis, Dynamic analysis and control of a Stewart platform manipulator, Journal of Robotic Systems 10 (5) (1993) 629–655.
- [9] L.W. Tsai, Solving the inverse dynamics of a Stewart–Gough manipulator by the principle of virtual work, Journal of Mechanical Design, Transactions of the ASME 122 (2000) 3–9.
- [10] H.E. Merritt, Hydraulic Control Systems, Wiley, 1967.
- [11] C.C. Nguyen, S.S. Antrazi, Z.L. Zhou, C.E. Campbell, Adaptive control of a Stewart platform-based manipulator, Journal of Robotic Systems 10 (5) (1992) 657–687.
- [12] N.I. Kim, C.W. Lee, High speed tracking control of Stewart platform manipulator via enhanced sliding mode control, in: IEEE Conference on Robotics and Automation, Belgium, 1998, pp. 2716–2721.
- [13] D. Garagic, K. Srinivasan, Application of nonlinear adaptive control techniques to an electrohydraulic velocity servo-mechanism, IEEE Transactions on Control Systems Technology 12 (2004) 303–314.

- [14] M.R. Sirouspour, S.E. Salcudean, Nonlinear control of hydraulic robots, *IEEE Transactions on Robotics and Automation* 17 (2) (2001) 173–182.
- [15] M. Honegger, P. Corke, Model-based control of hydraulic actuated manipulators, in: *Proceedings IEEE International Conference on Robotics & Automation*, Seoul, Korea, 2001, pp. 2553–2559.
- [16] I. Davliakos, E. Papadopoulos, Development of a model-based nested controller for electrohydraulic servos, in: *Proceedings 13th Mediterranean Conference on Control and Automation*, June 27–29, Limassol, Cyprus, 2005, pp. 107–112.
- [17] D. Li, S.E. Salcudean, Modeling, Simulation, and control of a hydraulic stewart platform, in: *Proceedings of the IEEE International Conference on Robotics and Automation*, 1997, pp. 3360–3366.
- [18] M.R. Sirouspour, S.E. Salcudean, A New approach to the control of a hydraulic stewart platform, in: *Proceedings of the 7th International Symposium on Experimental Robotics*, 2000, pp. 447–460.
- [19] D.H. Kim, J.Y. Kang, K.I. Lee, Robust tracking control design for a 6 DOF parallel manipulator, *Journal of Robotic Systems* 17 (10) (2000) 527–547.
- [20] B.A. Helouvyry, P. Dupont, C.C. De Wit, A survey of models, analysis tools and compensation methods for the control of machines with friction, *Automatica* 30 (7) (1994) 1083–1138.
- [21] D. Rowell, D.N. Wormley, Wormley, *System Dynamics: An Introduction*, Prentice Hall, 1997.
- [22] J.F. Blackburn, G. Reethof, J.L. Shearer, *Fluid Power Control*, MIT Press, Cambridge, MA, 1960.
- [23] W.J. Thayer, Specification standards for electrohydraulic flow control servovalves. Technical Bulletin 117, Moog Incorporation Control Division, E. Aurora, New York, 1962.
- [24] I.A. Bonev, J. Ryu, S.-G. Kim, S.-K. Lee, A closed-form solution to the direct kinematics of nearly general parallel manipulators with optimally located three linear extra sensors, *IEEE Transactions on Robotics and Automation* 17 (2) (2001) 148–156.
- [25] L. Baron, J. Angeles, The direct kinematics of parallel manipulators under joint-sensor redundancy, *IEEE Transactions on Robotics and Automation* 16 (1) (2000) 12–19.
- [26] W. Khalil, E. Dombre, *Modeling, identification & control of robots*, Hermes Penton Science, 2002.
- [27] L. Ljung, *System Identification – Theory for the User*, second ed., PTR Prentice Hall, New York, 1999.
- [28] D.H. Kim, J.-Y. Kang, Robust nonlinear observer for forward kinematics solution of a Stewart platform: an experimental verification, *Robotica* (18) (2000) 601–610.